Dependent and multiple scattering in transmission and backscattering optical coherence tomography

V. Duc Nguyen,[1] D. J. Faber,[1] E. van der Pol,[1] T. G. van Leeuwen,[1] and J. Kalkman[1,2,*]

[1] *Biomedical Engineering & Physics, Academic Medical Center, University of Amsterdam, P.O. Box 22700, Amsterdam 1100 DE, Netherlands*

[2] *Quantitative Imaging Group, Faculty of Applied Sciences, Delft University of Technology, Lorentzweg 1, 2628 CJ Delft, Netherlands*

[*] *j.kalkman@tudelft.nl*

Abstract: We use transmission and backscattering optical coherence tomography (OCT) to distinguish and quantify dependent and multiple scattering effects in turbid media. With transmission OCT the dependent scattering coefficients for a range of monodisperse silica particle suspensions are determined. An excellent agreement is observed between the measured dependent scattering coefficients and calculations based on Mie calculations, the Percus-Yevick radial distribution function, and coherent light scattering theory. Backscattering OCT measurements are fitted using the extended Huygens-Fresnel (EHF) model with the dependent scattering coefficients obtained from the transmission OCT measurements as input parameters. Good agreement between the EHF model and the backscattering OCT measurements is observed. For large particles, the rms scattering angle θ_{rms} obtained from the EHF fit is in fair agreement with θ_{rms} calculated from the transmission OCT data.

OCIS codes: (020.1670) Coherent optical effects; (170.4500) Optical coherence tomography; (290.4210) Multiple scattering; (290.7050) Turbid media.

References and links

1. N. Bosschaart, D. J. Faber, T. G. van Leeuwen, and M. C. G. Aalders, "Measurements of wavelength dependent scattering and backscattering coefficients by low-coherence spectroscopy," J. Biomed. Opt. **16**, 030503 (2011).
2. V. M. Kodach, D. J. Faber, J. van Marle, T. G. van Leeuwen, and J. Kalkman, "Determination of the scattering anisotropy with optical coherence tomography," Opt. Express **19**, 6131–6140 (2011).
3. J. Kalkman, R. Sprik, and T. G. van Leeuwen, "Path-length-resolved diffusive particle dynamics in spectral-domain optical coherence tomography," Phys. Rev. Lett. **105**, 198302 (2010).
4. N. Weiss, T. G. van Leeuwen, and J. Kalkman, "Localized measurement of longitudinal and transverse flow velocities using optical coherence tomography," Phys. Rev. E **88**, 042312 (2013).
5. R. K. Wang, "Signal degradation by multiple scattering in optical coherence tomography of dense tissue: a Monte Carlo study towards optical clearing of biotissues," Phys. Med. Biol. **47**, 2281–2299 (2002).
6. J. Kalkman, A. V. Bykov, D. J. Faber, and T. G. van Leeuwen, "Multiple and dependent scattering effects in Doppler optical coherence tomography," Opt. Express **18**, 3883–3892 (2010).
7. J. Kalkman, A. V. Bykov, G. J. Streekstra, and T. G. van Leeuwen, "Multiple scattering effects in Doppler optical coherence tomography of flowing blood," Phys. Med. Biol. **57**, 1907–1917 (2012).
8. L. Thrane, H. T. Yura, and P. E. Anderson, "Analysis of optical coherence tomography systems based on the extended Huygens-Fresnel principle," J. Opt. Soc. Am. A **17**, 484–490 (2000).

#195729 - $15.00 USD Received 13 Aug 2013; revised 30 Oct 2013; accepted 7 Nov 2013; published 18 Nov 2013

9. D. J. Faber and T. G van Leeuwen, "Are quantitative attenuation measurements of blood by optical coherence tomography feasible?, Opt. Lett. **34**, 1435–1437 (2009).
10. M. R. Hee, J. A. Izatt, J. M. Jacobson, J. G. Fujimoto, and E. A. Swanson, "Femtosecond transillumination optical coherence tomography," Opt. Lett. **18**, 950–952 (1993).
11. G. Singh and L. Song, "Influence of sodium dodecyl sulfate on colloidal fouling potential during ultrafiltration," Colloids Surf. A **218**, 138–146 (2006).
12. J. R. Zijp and J. J. ten Bosch, "Pascal program to perform Mie calculations," Opt. Eng. **32**, 1691–1695 (1993).
13. K. F. Palmer and D. Williams, "Optical properties of water in the near infrared," J. Opt. Soc. Am. **64**, 1107–1110 (1974).
14. M. Bass, C. De Cusatis, J. M. Enoch, V. Lakshminarayanan, G. Li, C. MacDonald, V. N. Mahajan, and E. Van Stryland, *Handbook of Optics*, 3rd ed. (McGraw-Hill, 2009), Vol. 4.
15. J. D. Cartigny, Y. Yamada, and C. L. Tien, "Radiative transfer with dependent scattering by particles: part 1 - theoretical investigation," J. Heat Transfer **108**, 608–613 (1986).
16. L. Hespel, S. Mainguy, and J. J. Greffet, "Theoretical and experimental investigation of the extinction in a dense distribution of particles: nonlocal effects," J. Opt. Soc. Am. A **18**, 3072–3076 (2001).
17. J. K. Percus and G. J. Yevick, "Analysis of classical statistical mechanics by means of collective coordinates," Phys. Rev. **110**, 1–13 (1958).
18. L. Tsang, J. A. Kong, K. H. Ding, and C. O. Ao, *Scattering of Electromagnetic Waves: Numerical Simulations* (Wiley, 2001).
19. J. M. Schmitt and A. Knüttel, "Model of optical coherence tomography of heterogeneous tissue," J. Opt. Soc. Am. A **14**, 1231–1242 (1997).
20. D. J. Faber, F. J. van der Meer, M. C. G. Aalders, and T. G van Leeuwen, "Quantitative measurement of attenuation coefficients of weakly scattering media using optical coherence tomography," Opt. Express , **12** 4353–4365 (2004).
21. H. T. Yura and S. G. Hanson, "Effects of receiver optics contamination on the performance of laser velocimeter systems," J. Opt. Soc. Am. A **13**, 1891–1902 (1996).
22. C. F. Bohren and D. R. Huffman, *Absorption and Scattering of Light by Small Particles* (Wiley, 1983).
23. G. Göbel, J. Kuhn, and J. Fricke, "Dependent scattering effects in latex-sphere suspensions and scattering powders," Waves Random Complex Medium **5**, 413–426 (1995).
24. A. Giusto, R. Saija, M. A. Iatì, P. Denti, F. Borghese, and O. I. Sindoni, "Optical properties of high-density dispersions of particles: application to intralipid solutions," Appl. Opt. **42**, 4375–4380 (2003).
25. G. Zaccanti, S. Del Bianco, and F. Martelli, "Measurements of optical properties of high-density media," Appl. Opt. **42**, 4023–4030 (2003).
26. E. C. C. Cauberg, D. M. de Bruin, D. J. Faber, T. M. de Reijke, M. Visser, J. M. C. H. de La Rosette, and T. G. van Leeuwen, "Quantitative measurement of attenuation coefficients of bladder biopsies using optical coherence tomography for grading urothelial carcinoma of the bladder," J. Biomed. Opt. **15**, 066013 (2010).
27. C. Xu, J. M. Schmitt, S. G. Carlier, and R. Virmani, "Characterization of atherosclerosis plaques by measuring both backscattering and attenuation coefficients in optical coherence tomography," J. Biomed. Opt. **13**, 034003 (2008).
28. L. Scolaro, R. A. McLaughlin, B. R. Klyen, B. A. Wood, P. D. Robbins, C. M. Saunders, S. L. Jacques, and D. D. Sampson, "Parametric imaging of the local attenuation coefficient in human axillary lymph nodes assessed using optical coherence tomography," Biomed. Opt. Express **3**, 366–379 (2012).

1. Introduction

Light scattering in turbid media such as the atmosphere, fluids, gels, paints, and tissue is of great importance in a wide variety of fields such as atmospheric science, astronomy, rheology, chemistry, forensics, biology, and medicine. Conventional light scattering techniques, such as static light scattering, dynamic light scattering, diffuse reflectance spectroscopy, and laser Doppler flowmetry, measure spatially averaged properties of scattering media. As a result, quantification of scattering properties is challenging in inhomogeneous and/or dense media.

The use of low coherence based techniques such as optical coherence tomography (OCT) and low coherence interferometry/spectroscopy allows for the path-length resolved measurement of light scattering properties inside samples. These techniques are based on a combination of confocal and coherence gated (path length resolved) light detection. By the combination of the two gating techniques a strong rejection of multiple scattered light is achieved and mainly single scattered light is detected. As a result, for samples consisting of a dilute ensemble of particles, the measured OCT signal can be well described by a single and independent scattering model.

#195729 - $15.00 USD Received 13 Aug 2013; revised 30 Oct 2013; accepted 7 Nov 2013; published 18 Nov 2013

Based on this model local quantitative measurement of static [1, 2] and dynamic [3, 4] light scattering properties has been performed. However, in high scattering media both the single and the independent scattering assumption can be invalid.

For high scattering media that consist of a dense ensemble of single particles (e.g. colloidal suspensions), interference effects between the waves scattered from the different particles can take place if the inter-particle separation is small. As a result, the scattering strength is reduced and the scattering phase function is modified. In OCT, concentration dependent scattering can result in a reduction of the measured signal attenuation in depth compared to the independent particle model.

Although OCT efficiently collects mainly single scattered light, for high scattering media multiple scattered light can have a profound effect on the OCT signals. From OCT measurements and Monte Carlo (MC) simulations it has been shown that, compared to the single scattering description, multiple scattering leads to a reduced axial resolution [5], underestimation of the scattering coefficient and a distortion of the Doppler OCT flow profile [6, 7]. Consequently, the presence of multiple scattering makes accurate quantification of any light scattering property based on the OCT signal challenging.

An analytical model of the OCT signal has been developed based on the extended Huygens-Fresnel (EHF) principle that includes the effect of multiple scattering [8]. This model describes the OCT signal in depth and is based on the assumption of small angle (multiple) scattering. The model parameters are the scattering coefficient and the root mean square (rms) scattering angle, which is related to the scattering phase function. These two parameters have been shown to be highly correlated in fits of the OCT signal using this model [9]. Moreover, this model does not incorporate the effect of concentration dependent scattering and is therefore based on a priori unknown optical parameters. Consequently, it is very difficult to validate this model, disentangle dependent from multiple scattering, and quantify both effects using backscattering OCT only.

Here, we present a solution to this problem by combining the information obtained from backscattering and transmission OCT [10]. In transmission OCT the effect of multiple scattering on the optical transmission is eliminated by the use of low-coherence path-length-resolved detection of ballistic (unscattered) light. From these measurements the concentration dependent scattering coefficient is determined and compared to an analytical model. The backscattering OCT data is then fitted with the analytical EHF model using the measured dependent scattering coefficient as input.

2. Materials and methods

2.1. Sample preparation

Colloidal suspensions with monodisperse silica beads of different diameters are prepared and characterized before OCT measurement. Silica beads (Kisker Biotech, Steinfurt, Germany) in powdered form are weighted and suspended in de-ionized water. Sodium dodecyl sulfate is added in a solution of 0.3 mM to prevent aggregation [11]. The resulting suspensions are vortexed for 60 minutes and sonicated for 15 minutes. To determine the particle size distributions, the solutions are diluted in deionized water to a concentration between 10^7 and 10^8 beads per mL and allowed to adhere to formvar-carbon coated 300 mesh grids (Electron Microscopy Sciences, Hatfield, USA). After complete water evaporation, the beads are imaged with a transmission electron microscope (Philips CM-10) operating at 100 kV. From at least 635 beads, for every particle diameter, the surface area for every particle is determined using the Analyze Particles function in ImageJ software. Subsequently, the diameter of each bead is calculated from the surface area and used in the particle size distribution. The particle size distributions are fitted by Gaussian functions to obtain the mean diameter and standard deviation. Figure 1

#195729 - $15.00 USD Received 13 Aug 2013; revised 30 Oct 2013; accepted 7 Nov 2013; published 18 Nov 2013

shows the typical particle size distribution and the transmission electron micrograph (inset) of silica beads with a diameter of 376±20 nm. Table 1 summarizes the obtained mean diameters, standard deviations, and maximum volume concentrations of the used silica beads. Before OCT measurements, the suspensions are vortexed for 10 minutes and sonicated for 10 minutes to prevent particle aggregation.

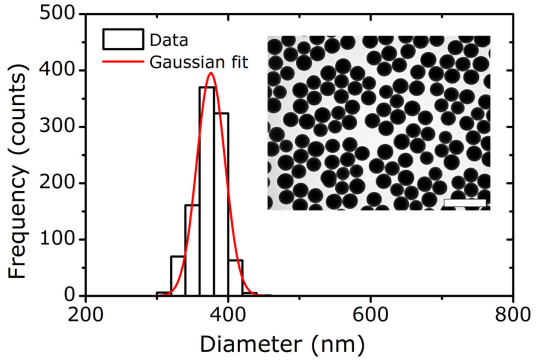

Fig. 1. Size distribution of Psi-0.5 silica particles measured with transmission electron microscopy (inset) and the corresponding Gaussian fit. The fit yields a mean diameter of ϕ=376 nm and a standard deviation of 20 nm.

Table 1. Catalog number, mean diameter, standard deviation, and maximum volume concentration of silica beads. Scattering cross section and anisotropy factor g_s are obtained from Mie theory.

Cat.#	mean diameter [nm]	st. dev. [nm]	max. vol.%	σ_s (Mie) [μm^2]	g_s (Mie)
Psi-1.5	1215	18	10	0.24026	0.869
Psi-1.0	906	17	10	0.069361	0.781
Psi-0.8	759	14	20	0.031297	0.742
Psi-0.5	376	20	20	0.0012451	0.253

2.2. Calculations

2.2.1. Mie calculations

Mie calculations of the scattering cross section σ_s and phase function $p_{Mie}(\theta)$ are performed with home written code based on publicly available code [12]. The diameter of the particles is determined from the transmission electron microscopy measurements as shown in Table 1. The calculations are based on the OCT center wavelength λ=1.297 μm (the effect of the bandwidth of the light source is negligible). The refractive index of water is used as the refractive index of the medium n_{med}=1.324 [13]. The refractive index of the silica particle is optimized to match the scattering coefficients obtained from the transmission OCT measurements for all particle sizes and concentrations and is n_{part}=1.441, which is close to the value from literature n=1.447 [14]. The scattering coefficient μ_s is calculated from σ_s by multiplying with the particle concentration for a particular particle suspension. In the Mie calculations we assume the incident light to have isotropic polarization, i.e. $p_{Mie}(\theta)$ is the average over the two orthogonal polarizations.

#195729 - $15.00 USD Received 13 Aug 2013; revised 30 Oct 2013; accepted 7 Nov 2013; published 18 Nov 2013

2.2.2. Dependent scattering calculations

For high particle concentrations far field interference effects take place that lead to a reduction in the scattering efficiency. These interference effects are described by the structure factor $S(f_v,\theta)$. Following the work of Cartigny et al. [15] and Hespel et al. [16], the ratio of dependent over independent scattering efficiency for varying volume fraction is calculated with

$$\frac{Q_{dep}(f_v)}{Q_{Mie}} = 2\pi \int_0^{\pi} S(f_v,\theta) p_{Mie}(\theta) \sin\theta d\theta, \tag{1}$$

where $p_{Mie}(\theta)$ is the normalized phase function determined from Mie calculations and $S(f_v,\theta)$ is the structure function dependent on volume fraction f_v and scattering angle θ. For point source particles the structure factor $S(f_v,\theta)$ is calculated by

$$S(f_v,\theta) = 1 + 24 f_v \int_0^{\infty} R^2 (g(R)-1) \frac{\sin(q\phi R)}{q\phi R} dR, \tag{2}$$

with $R = r/\phi$, r a radial variable, ϕ the particle diameter, $g(R)$ the radial distribution function, and the scattering vector $q = 4\pi n_{med} sin(\theta/2)/\lambda$. Equation (2) is based on the assumption of point scatterers, i.e. that the phase change across the particle is small. This is summarized by the so-called extended Rayleigh-Debye condition

$$2x \left| \frac{n_{part}}{n_{med}} - 1 \right| \ll 1, \tag{3}$$

with x the size parameter $x = \pi\phi n_{med}/\lambda$ and n_{part} the refractive index of the particle. Finally, the concentration dependent phase function is calculated according to

$$p_{dep}(\theta) = \frac{Q_{Mie}}{Q_{dep}} S(f_v,\theta) p_{Mie}(\theta). \tag{4}$$

The radial distribution function $g(R)$ describes the probability of finding a particle at a certain distance from another particle. For $g(R)$ we use the Percus-Yevick (P-Y) model [17], which takes into account interactions between particles (i.e. spatial correlations between the particle positions). The short range interactions cause the particles not to penetrate each other, i.e. $g(R) = 0$ for $R < 1$, the long(er) range inter-particle forces lead to variations in $g(R)$ around unity for $R > 1$. The P-Y potential is calculated using the formalism described in [18]. From the P-Y potential, the structure factor is calculated using Eq. (2), while ensuring that for all calculations $S(f_v,\theta) > 0$, i.e. only physical solutions exist. The structure factor, in combination with the phase function, is used in the numeric integration of Eq. (1), which results in a calculation of the scattering efficiency ratio. To compare the measurements of μ_s with the dependent scattering calculations, the calculated scattering efficiency ratio is multiplied with the Mie scattering coefficient, i.e. $\mu_{s,dep} = Q_{dep}\mu_s/Q_{Mie}$.

The scattering anisotropy g_s, defined as the average cosine of the scattering angle, is calculated in the usual way from $p_{dep}(\theta)$ after normalization. Hence, the scattering anisotropy g_s varies with volume fraction and is also concentration dependent.

2.2.3. Extended Huygens-Fresnel model of the backscattering OCT signal

The influence of multiple scattering on the backscattering OCT signal is described by the model proposed by Schmitt et al. [19] and Thrane et al. [8] that is based on the extended

#195729 - $15.00 USD Received 13 Aug 2013; revised 30 Oct 2013; accepted 7 Nov 2013; published 18 Nov 2013

Huygens-Fresnel (EHF) formalism. In this model the sample beam propagates through the random medium and the mean square signal current collected from depth z is described as a contribution of three terms: the single-backscattered field, the field that is subject to multiple (forward) scattering while propagating, and a coherent cross term:

$$i(z)^2 \propto exp(-2\mu_s z) + \frac{2exp(-\mu_s z)[1-exp(-\mu_s z)]}{1+\frac{w_s^2}{w_h^2}} + [1-exp(-\mu_s z)]^2 \frac{w_h^2}{w_s^2}, \tag{5}$$

where μ_s is the (dependent) scattering coefficient, w_h is the beam waist in the absence of scattering, w_s is a beam waist that increases with propagation length due to (multiple) scattering (e.g. accounting for lateral resolution loss in scattering media).

Single backscattering, which is one contribution to the EHF model, assumes a single point reflection at the location of the coherence gate in the sample and otherwise an undisturbed propagation of the sample field. Whereas the coupling efficiency of the single backscattered field is quantified with the beam waist w_h [20], for the multiple scattering contribution to the OCT signal an additional geometrical parameter w_s is present because the lateral coherence length ρ_0 of the scattered field increases as the wave propagates through the sample (the so-called shower curtain effect). The lateral coherence length characterizes the phase fluctuation length scale of the scattered wavefront, with larger ρ_0 meaning larger contributions to the signal. Under the approximation that $sin\theta \approx \theta$, ρ_0 is inversely proportional to the root-mean-square scattering angle θ_{rms}. Consequently, as the scattering anisotropy g_s goes up, so does ρ_0 and so does the multiple scattering contribution. The aforementioned approximation implies that the analytical result in Eq. (5) is only valid for small angle scattering, i.e. small θ_{rms}. The root-mean-square scattering angle θ_{rms} is calculated from the phase function $p_{dep}(\theta)$ according to [21]

$$\theta_{rms} = \sqrt{\frac{\int_0^\pi \sin^2\theta\, p_{dep}(\theta)\sin\theta d\theta}{\int_0^\pi p_{dep}(\theta)\sin\theta d\theta}}. \tag{6}$$

The practical use of the EHF fit model without any a priori knowledge of sample related input parameters is difficult since the model is over-parameterized as μ_s and θ_{rms} are correlated [9]. As a result, a change in one value can be compensated by a change in the other without reducing the fit statistics (e.g. χ^2). We fit the backscattering OCT signal using the EHF model with the addition of an amplitude fit parameter, but with μ_s obtained from the transmission OCT data. Hence, θ_{rms} is the only OCT slope related fit parameter. In our analysis we neglect optical absorption (μ_a=0.135 mm^{-1} at λ=1300 nm)

2.3. Experimental OCT set-ups

For backscattering OCT a home built spectral-domain OCT system is used as shown in Fig. 2(a) [6]. The light source (B&W Tek superluminescent diode) has a center wavelength λ_c = 1.297 μm and a full width at half maximum bandwidth of $\Delta\lambda$ = 40 nm. Light from the source is coupled into a 90/10 fiber coupler, with 90% of the light to the sample arm and 10% to the reference arm. Light from the sample and reference arm is directed, using a circulator, towards a spectrometer with a 46 kHz linescan camera as detector (Sensors Unlimited SU-LDH-1.7RT/LC). The OCT signal is obtained from the spectra after resampling and through an inverse Fourier transformation.

For the backscattering OCT measurements, the silica particle solution is contained in a cuvette of 450 μm thickness. The cuvette is aligned such that the focus is a the first interface, The backscattering OCT data is averaged ($\sim$ 10000 A-scans), its background is subtracted, corrected for SD-OCT roll-off, corrected for confocal point spread function, and subsequently

#195729 - $15.00 USD Received 13 Aug 2013; revised 30 Oct 2013; accepted 7 Nov 2013; published 18 Nov 2013

fitted with the EHF model as described by Eq. (5). The fit model features three parameters: an amplitude for scaling, μ_s, and θ_{rms}. The EHF fits to the backscattering OCT data use μ_s from the transmission measurements as fixed parameter, leaving only two free running variables. The uncertainty in the fit parameter is estimated by repeating the measurement 5 times.

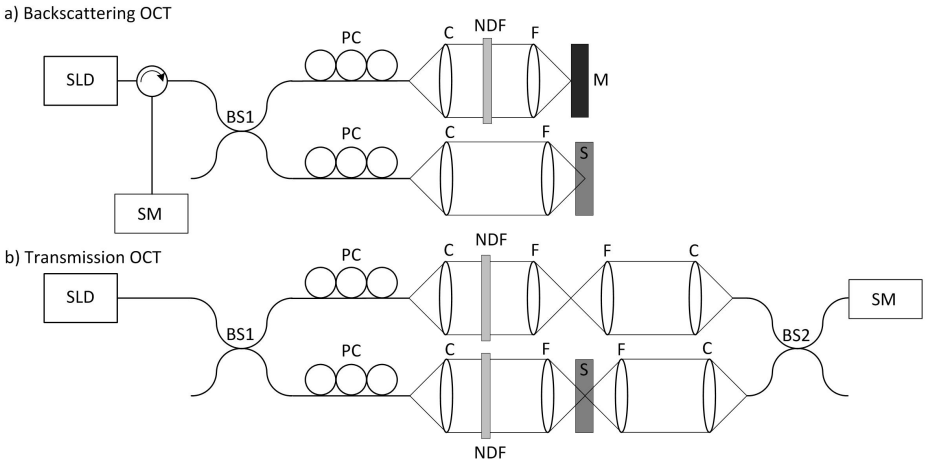

Fig. 2. Experimental setup for backscattering (a) and transmission (b) SD-OCT. SLD: super luminescent diode, BS1: 90:10 fiber splitter, BS2: 50:50 fiber splitter, PC: polarization control, C: achromatic lenses, NDF: neutral density filter, SM: spectrometer, M: mirror, S: sample.

Transmission OCT measurements are performed using a modified version of the backscattering OCT system based on a Mach-Zehnder interferometer to measure the path-length resolved optical transmission, as shown in Fig. 2(b). Light is coupled into the fiber coupler with 90% going to the sample arm and 10% going to the reference arm. Identical optical components are used in sample and reference arm to reduce any effects of dispersion. For optical power control, neutral density filters are placed in both arms. In sample and reference arm, light is collimated using an autocollimator and thereafter passes two focusing achromatic lenses (NA = 0.04). The light is collected by another collimator and coupled in the 50:50 fiber coupler, and guided to the spectrometer.

For the transmission OCT measurements, the silica particle solution is contained in a cuvette with 1 mm path length through the solution, which is aligned to be in the center of 2 focusing achromatic lenses. Exchange of the solution in the cuvette is performed using a syringe without movement of the cuvette. It is checked that before and after a measurement the alignment of the transmission has not varied as the transmitted powers in sample and reference arm are equal to before the measurement. A single measurement is the average of 100.000 transmission scans.

The scattering coefficient (μ_s) is determined from the ballistic (non-scattered) light in the transmission OCT signal according to the following steps:

1. Determine the peak magnitude of the OCT signal through the 1 mm cuvette containing de-ionized water: $|a_{water}|$
2. Determine the peak magnitude of the OCT signal of ballistic light through a 1 mm cuvette containing the silica particle solution: $|a_{sol}|$
3. Calculate the scattering coefficient of the silica particle solution based on the law of Lambert-Beer:

$$\mu_s = ln\frac{|a_{water}|^2}{|a_{sol}|^2} \tag{7}$$

#195729 - $15.00 USD Received 13 Aug 2013; revised 30 Oct 2013; accepted 7 Nov 2013; published 18 Nov 2013

The uncertainty in μ_s is estimated by taking the standard deviation of $|a_{water}|$ and $|a_{sol}|$. Subsequently, the total error is calculated for μ_s. This procedure is followed for all particle sizes and concentrations.

3. Results

3.1. Transmission OCT

Figure 3 shows a typical set of averaged transmission OCT measurements for the 1215 nm diameter silica particles at varying volume concentration. A transmission peak can be observed at an optical path length of 450 μm. This transmission peak represents non-scattered light that has traveled the shortest distance through the sample, i.e. ballistic light. The width of the ballistic transmission peak is determined by the bandwidth of the light source and, for all concentrations, equals the bandwidth limited resolution of 17 μm. The height of the ballistic peak $|a_{sol}|$ represents the amount of ballistic light transmitted through the sample and decreases with increasing volume concentration of scatterers. Also indicated is the reference transmission of water $|a_{water}|$ and the peak magnitude of the ballistic transmission. At larger optical path lengths, a distribution of light can be observed, which corresponds to the multiple scattered light through the sample. The amount of multiple scattered light increases with increasing volume concentration of scatterers. At the highest volume concentration of scatterers (10 vol.%) the ballistic light cannot be observed.

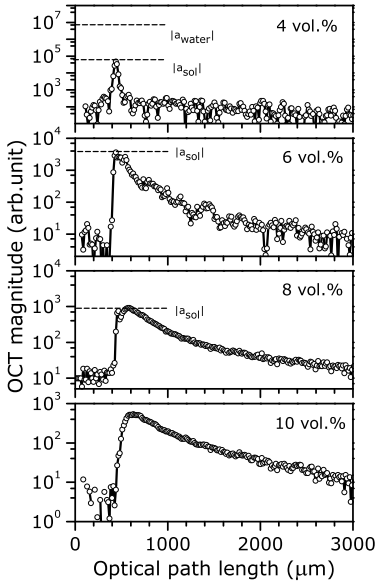

Fig. 3. Measured OCT signal versus optical path length in transmission OCT for ϕ= 1215 nm silica particles at varying volume concentrations (indicated). The dashed horizontal lines indicate $|a_{water}|$ and $|a_{sol}|$.

From the transmission measurements presented in Fig. 3 the scattering coefficient μ_s is determined for all particle diameters and concentration ranges as presented in Table 1. In Fig. 4 the measurements are compared to Mie calculations and dependent scattering calculations based on the P-Y potential. The measurement errors in μ_s and in the volume fraction are smaller than the symbols. Good agreement between the measurements and the dependent scattering calculations is obtained for a particle refractive index of n_{part}=1.441. From the dependent scattering calculations the concentration dependent scattering anisotropy g_s is calculated and presented in the lower panels of Figs. 4(a)–4(d). For large particles the relative change in scattering anisotropy

#195729 - $15.00 USD Received 13 Aug 2013; revised 30 Oct 2013; accepted 7 Nov 2013; published 18 Nov 2013

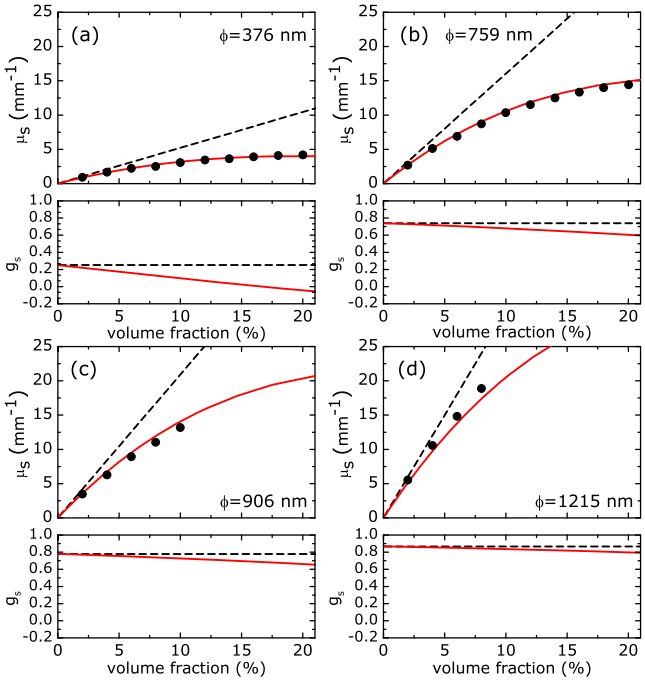

Fig. 4. Measured scattering coefficients for (a) 376 nm (b) 759 nm (c) 906 nm and (d) 1215 nm diameter particles. Mie (dashed black lines) and dependent scattering (solid red line) calculations of the scattering coefficient and the scattering anisotropy g_s are shown.

is small, however for small particles a large change in g_s can be observed. For the smallest particle diameter (ϕ=376 nm), g_s even becomes negative at large volume fractions.

3.2. Backscattering OCT

The good agreement between the transmission OCT data and the analytical dependent scattering model based on Mie calculations and the P-Y radial distribution function demonstrates that the effect of dependent scattering is well understood. The exact knowledge of the optical properties μ_s and $p_{dep}(\theta)$ of these samples give us the opportunity to validate the EHF model on the backscattering OCT signal with only the amplitude and θ_{rms} as fit parameters. The EHF model is suited for high g_s scattering, hence we validate the EHF model primarily for the $\phi = 1215$ nm particles.

Figure 5 shows OCT measurements in the backscattering geometry for $\phi = 1215$ nm diameter particles for varying volume concentration. The EHF model is fitted to the backscattering OCT data and describes the measured data very accurately for a large depth range in the cuvette. Also shown is the single scattering contribution to the backscatter OCT signal, i.e. the first term in Eq. (5). The single scattering contribution is dominant for small depths, however, for large depths, the single scattering model cannot describe the data very well and multiple scattering dominates the backscatter OCT signal. The difference between the single scattering contribution and the EHF fit is due to multiple scattering only and therefore is quantified as well.

The average scattering angle θ_{rms} obtained from the EHF fits to the OCT backscatter data are compared to θ_{rms} obtained from the dependent phase function originating from the transmission OCT measurements (Fig. 4). The result is shown in Table 2 for $\phi = 1215$ nm. In general, θ_{rms} from the EHF-model fit increases for increasing volume fraction, in agreement with the

#195729 - $15.00 USD Received 13 Aug 2013; revised 30 Oct 2013; accepted 7 Nov 2013; published 18 Nov 2013

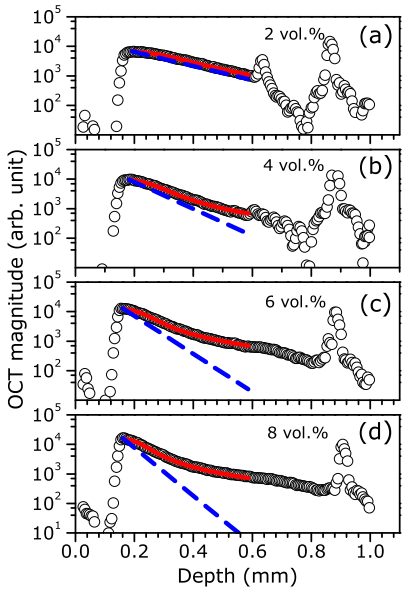

Fig. 5. Measured OCT signal versus depth in backscattering geometry for ϕ= 1215 nm silica particles at varying volume fractions (indicated). The solid red line indicates the EHF model fit, the dashed blue line indicates the single scattering contribution to the OCT backscatter signal.

reduction in g_s as shown in Fig. 4(d). The quantitative agreement between θ_{rms} derived from modeling the transmission OCT data and θ_{rms} from the fit of the backscattering OCT measurements is within approximately 10%. EHF fits are also performed on backscattering OCT data for ϕ=376 nm, ϕ=759 nm, and ϕ=906 nm, which are particle size for which θ_{rms} is outside the application range for the EHF model [8]. In general, the EHF fits to the backscatter OCT data become worse at smaller particles sizes (data not shown). For ϕ=376 nm and ϕ=759 nm, fit convergence is poor and the fit estimate of θ_{rms} is significantly lower than the analytical result.

Cat.#	mean diameter [nm]	vol.%	θ_{rms} (theory) [rad]	θ_{rms} (fit) [rad]
Psi-1.5	1215	8	0.58	0.64 ± 0.04
Psi-1.5	1215	6	0.57	0.59 ± 0.04
Psi-1.5	1215	4	0.56	0.58 ± 0.04
Psi-1.5	1215	2	0.55	0.49 ± 0.04

Table 2. Average scattering angle θ_{rms} for ϕ=1215 nm from the theory based on the transmission OCT data and from the EHF fits of the backscattering OCT data.

4. Discussion

We observed excellent agreement for the transmission OCT signals using our model based on Mie theory, the Percus-Yevick radial distribution function, and coherent scattering theory. For backscattering OCT on high scattering media a strong multiple scattering contribution is observed and agreement is found with the extended Huygens Fresnel model.

#195729 - $15.00 USD Received 13 Aug 2013; revised 30 Oct 2013; accepted 7 Nov 2013; published 18 Nov 2013

4.1. Transmission OCT

In this work we used transmission OCT to estimate the effect of dependent scattering on μ_s and θ_{rms}. We observe a good agreement between the measurements and the analytical theory in Fig. 4 for all particle diameters. Although the extended Rayleigh-Debye condition (Eq. (3)) is not strictly obeyed for the largest particles, the good agreement is to be expected since for the forward direction Mie calculations give results that are similar to that for larger spherical particles (the spherical particle form factor is unity around zero scattering angle [22]). The largest uncertainty in the application of this model is in the refractive index of the silica particles. Even for small deviations on n_{part}=1.441, the theoretical predictions deviate from the experimental results. Additional measurements are necessary for an accurate and independent determination of the particle refractive index.

The general trend in dependent scattering of a lowered scattering efficiency with increasing particle volume fraction as observed in our measurements is similar to observations using other light scattering methods, for example: Göbel et al. [23], Giusto et al. [24], and Zaccanti et al. [25]. Moreover the observed decrease of the scattering anisotropy with increasing volume fraction is similar to that observed for Intralipid [25].

The maximum optical thickness that we could measure in transmission OCT is around 20 mean free paths (MFP) for ϕ=1215 nm. At this large optical thickness it is possible to measure up to even higher volume fractions for smaller particles as these smaller particles have a lower scattering cross sections. However, the biggest experimental challenge is to make high concentration suspensions of monodisperse particles that do not suffer from particle aggregation and/or sedimentation. In the future, using higher sample arm powers and using a smaller coherence length light sources, the detection and discrimination of ballistic and multiple scattered light can further improve. Consequently, we anticipate a further improvement of the 20 MFP transmission imaging depth and allow for the measurement of dependent scattering effects at even larger volume fractions, i.e. smaller inter-particle distances.

The combination of the presented technique with parameters obtained from other OCT-based methods measurements, such as the particle diameter, particle diffusion [3], particle flow [4], and scattering anisotropy [2] result in a powerful platform to measure optical properties of colloidal suspensions. As we have shown here, the detailed knowledge of the optical properties gives access to the microrheology of the colloidal particles as described by the radial distribution function. Using improved control over the particle-particle interactions, e.g. by changing the charge distribution between the particle and the solutes, transmission OCT can be an excellent platform to study the effect particle-particle interactions on the radial distribution function.

Finally, we point out that in diffuse optical transmission measurements it is $\mu_s' = \mu_s(1-g_s)$ that typically determines the amount of light that is transmitted. As can be observed from Fig. 4, the concentration dependency of μ_s' is expected to be weaker due to the opposing effects of μ_s and g_s on concentration. Hence, we expect that these effects are more difficult to observe in diffuse optical transmission experiments.

4.2. Backscattering OCT

The correct fitting of the EHF model to the backscattering OCT data using an independently determined input parameter is a strong validation of this over-parametrized OCT model. Furthermore, by comparing the EHF model fit with the single scattering contribution, the amount of multiple scattering in the OCT signal is quantified by the difference between the two. Although, in this experiment, the magnitude of the OCT signal in depth is quantified, it is still to be investigated both in experiment and in theory what the influence of multiple scattering is on the OCT image quality for biological tissue. For example, it is still unknown how multiple scattering affects the OCT imaging depth, the OCT image contrast, and the axial resolution.

#195729 - $15.00 USD Received 13 Aug 2013; revised 30 Oct 2013; accepted 7 Nov 2013; published 18 Nov 2013

Our analysis demonstrates that the relation between the slope of the OCT signal in depth and the attenuation coefficient is complex. Although biological tissue does not consist of individual particles, but rather a continuous distribution of refractive index variations, the effect of disease state is regularly quantified based on the OCT attenuation coefficient in a number of studies [26, 27, 28]. The value of our work for these studies is that the use of a more advanced model, which takes into account the effect of multiple scattering, can lead to a more accurate determination of the optical properties of tissue. Although, the correct fitting of these models to the data requires additional information, as we we have shown, this information can be obtained from the height of the OCT signal [2] or from spectrally resolved measurements [1]. We expect that the application of these more advanced OCT signal models in clinical light scattering studies can improve the diagnostic value of these optical biopsies.

5. Conclusion

In conclusion, we have shown measurements of concentration dependent scattering coefficients using transmission OCT that are in good agreement with analytical theory. Based on the measured concentration dependent scattering coefficients we validated the EHF model of the backscattering OCT signal for large particles.

Acknowledgments

This work was supported by the Smart Mix Program of the Netherlands Ministry of Economic Affairs and the Netherlands Ministry of Education, Culture and Science and the IOP Photonic Devices program managed by the Technology Foundation STW and Agentschap NL.

#195729 - $15.00 USD Received 13 Aug 2013; revised 30 Oct 2013; accepted 7 Nov 2013; published 18 Nov 2013